PCCP

Accepted Manuscript

ROYAL SOCIETY OF CHEMISTRY

www.rsc.org/pccp

Journal Name

ARTICLE

Ether and Siloxane Functionalized Ionic Liquids and their Mixtures as Electrolyte for Lithium-ion Batteries

Received 00th January 20xx,
Accepted 00th January 20xx

DOI: 10.1039/x0xx00000x

www.rsc.org/

Santosh N. Chavan, Aarti Tiwari, Tharamani C. Nagaiah* and Debaprasad Mandal*

The present study deals with an investigation of two novel imidazolium ionic liquids bearing ether-ether (1O2O2-Im-2O1) and ether-siloxane (1O2O2-Im-1SiOSi) functionalities with TFSI anion and their mixtures with propylene carbonate as electrolyte in lithium-ion battery. The electrochemical stability and conductivity of these novel ILs were analyzed by electrochemical studies such as cyclic voltammetry, linear sweep voltammetry and impedance measurements. The applicability of these ILs as an electrolyte in Li-ion batteries was studied in presence of high concentration of LiTFSI (1 mol/kg electrolyte) and ether-ether IL was shown to possess high electrochemical stability window (ESW) of 5.9 V and good conductivity of 2.2 mS/cm. The electrochemical stability and conductivity was further complimented by self-diffusion of different ions using pulsed gradient spin-echo (PGSE) NMR, viscosity and thermal properties like TGA and DSC analysis. More importantly, we explored the effect of temperature on the electrochemical stability and conductivity of these ILs by electrochemical impedance spectroscopy.

1 Introduction

Electrochemical batteries have eventually become the appraised choice owing to its high conversion efficiency without effluent emission.[1] Among the present rechargeable batteries, lithium and lithium-ion batteries exhibit the highest energy density.[2-6] Provided its huge applicability, there is an intense drive towards their betterment for achieving even higher power and energy dense systems.[7] Presently research is ongoing towards advancement of its various components like anode, cathode and electrolyte.[3-5] The recital of a battery depends on various parameters which include the conductivities of the electrodes, electrochemical potential window of electrolyte (redox reaction at the cationic and anodic counter part of the reaction) and Li-insertion into the electrode. More importantly, the battery performance relies upon electrochemical stability of the electrolyte, as it facilitates ion transport conferring efficient rechargebility and governs its overall stability.[8] Low flash-point of conventional electrolyte systems restrains usage of high energy electrodes to achieve desired output energy level, compromising both power density and safety.[6]

Conventionally alkyl carbonates are employed in lithium and lithium-ion batteries as electrolytes to shuttle Li-ions back-and-forth between the two electrodes. These organic molecular solvents exhibit low viscosity and hence appreciable ionic conductivity of the dissolved Li-ions. Besides conducting Li-ions these also tend to react with the new-fangled high energy electrodes at the operation voltage which might cause localized overheating effecting subsequent thermal runaways hampering the obtainable specific capacity by the battery.[9] The aforesaid is many a times assisted by side reaction products reacting at the opposite electrode upon transportation and dendritic growth of lithium.[4,7, 10] These are usually averted partially upon successive cycling accompanied by passivation layer formation termed solid electrolyte interface (SEI) over either anode or cathode and sometimes both depending upon their respective composition.

Another impelling issue regarding electrolytes originates with the co-intercalation of conventional ones along with the Li-ions in the graphite electrode.[1, 5] These during discharge cycle tend to exfoliate the graphite with associated thermal effects posing serious concerns. The abovementioned crisis prevails on account of high volatility and flammability of conventional electrolytes unable to withstand high potentials causing undesired side reactions raising safety concerns towards commercialization and utilization at large scale. Hence, lots of researches are devoted for the search for alternative electrolytes. In recent years ionic liquids (ILs) have attracted an enormous attention not only in sustainable synthesis as green solvent, high temperature lubricants but also in electrochemical energy storage devices due to its tunable

S.N. Chavan, A. Tiwari, Dr. T.C. Nagaiah, Dr. D. Mandal
Department of Chemistry
Indian Institute of Technology Ropar
Rupnagar, Punjab-140001, India
E-mail: dmandal@iitrpr.ac.in
Electronic Supplementary Information (ESI) available: [details of any supplementary information available should be included here]. See DOI: 10.1039/x0xx00000x

properties, non-volatile, non-flammable, high thermal-electrochemical stability, high ionic conductivity and their ability to dissolve a wide variety of compounds.[11-13] These fluidic salts are marked by weak interactions between the asymmetric cation and the electronically diffused anion conferring the ILs their unique aspect of low crystallization tendency. Apart from the above mentioned features, applicability in electrochemical sphere obliges it to exhibit considerable conductivity (low viscosity) and wide potential range of stability (usually > 4 V). These features are in marked contrast with the conventional organic molecular solvents presently in practice. Due to their intrinsic nature of being molten salts with high ionic content, they could be conveniently substituted for the commonly employed electrolyte systems. These ILs could also be used in conjunction with the conventional carbonate-based electrolytes as blended systems.[14-17] This alternative takes care of the cost-effectiveness, while conferring enhanced ionic strength, reduced flammability and solid electrolyte interface (SEI) stability. The scientific community is thus looking forward towards the successful replacement of conventional electrolytes by ILs. More importantly, one can amend the conductivity and suitable electrochemical window by tuning cation and anion which are highly essential for the electrochemical storage devices such as Li ion batteries.

Among a vast pool of possible ILs, imidazolium-based ILs are quite popular due to its easy synthesis, favorable melting point, robustness against moisture and temperature while simultaneously being cost-effective and electrochemically stable.[12,17] The bis(trifluoromethanesulfonyl)imide (TFSI) anion in amalgamation with imidazolium cation unveils desirable features like low melting point, high thermal stability and ability to withstand a wide range of potential [12]. High viscosity (η) of ILs has been a major concern for their use as electrolytes, since they act as charge carrying species in electrochemical reactions and devices. But still they could be fine-tuned by suitably choosing the cationic and anionic constituents and functionalizing them appropriately.

To the best of our knowledge, the reported literature on lithium transport properties of IL-solvent mixture, either focused on IL-based electrolyte or mixture of IL and Li salt. Recently, mixture of ILs and conventional organic solvent based electrolytes have been reported to overcome the Li-ion transport limitation of IL based electrolytes while retaining a lower flammability than that of conventional electrolytes.[18-20] However, the ILs reported are only [Pyr]TFSI or alkylimdazolium cation[18-20] which are small cations and no functionality has been induced for Li-ion transportation, wherein the conductivity reported was very low although the Li salt (0.3 M) concentration is low compared to the concentration used in conventional electrolyte.

Hence, the present paper aims to bring forth two ILs bearing ether-ether (1O2O2-Im-2O1) and ether-siloxane (1O2O2-Im-1SiOSi) functionalities over imidazolium cation in order to probe the effect of cation with TFSI anion (Scheme 1) for application in lithium-ion batteries as electrolyte. Our previous study corroborated that ether-ether and ether-siloxane functionalized ILs have a wide liquid temperature range with suitably subtle viscosities even with high molecular weight bearing a bulky cation.[21] This is the first instance where the functionality was introduced to both the sides of imidazolium cation for better control over the thermophysical properties. Recently, few literatures have been reported on siloxane functionalized materials for energy applications. [22,23]

Here we intend to study the actual scenario, in terms of conductivity and electrochemical stability of these novel ILs using three-electrode system through detailed electrochemical studies which includes cyclovoltammetry (CV), linear sweep voltammetry (LSV) and electrochemical impedance spectroscopy (EIS) at various temperatures.

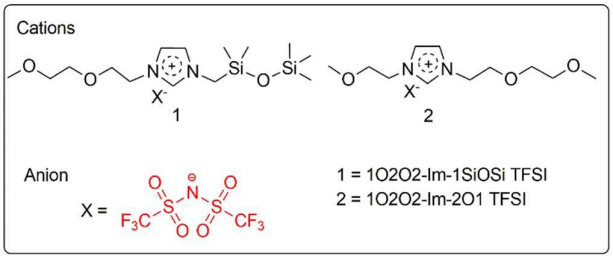

Scheme 1. Ionic Liquids used in this study.

In order to have an electrochemical benchmark test for Li ion batteries, we have further studied these aspects for neat ILs, mixture of IL and propylene carbonate (PC), and composite of the IL, PC and lithium bis(trifluoromethanesulfonyl)imide (LiTFSI). Each of these electrolytes was also individually assessed for physical properties like viscosity, liquid temperature range and thermal stability towards better understanding of these ILs and their rational ability to be employed as electrolytes in lithium and lithium-ion battery systems using thermogravimetric analysis (TGA), differential scanning calorimetry (DSC), infrared spectroscopy (IR) and pulsed gradient spin-echo (PGSE) NMR.

Table 1. Mole fraction of the investigated electrolytes.

Electrolytes	Mole fraction /mol%		
	IL	PC	Li
Ether-ether IL + PC	47.62	52.37	……
Ether-ether IL + PC + LiTFSI	36.92	40.62	22.44
Ether-ether IL + LiTFSI	66.89	…..	33.10
Ether-siloxane IL + PC	47.62	52.37	……
Ether-siloxane IL + PC + LiTFSI	35.40	38.96	25.63
Ether-siloxane IL + LiTFSI	62.05	…..	37.95

2 Experimental

2.1 Preparation of electrolytes

The 1O2O2-Im-2O1 TFSI and 1O2O2-Im-1SiOSi TFSI ILs were synthesized and characterized as per our previously reported literature. Briefly, the synthesis of ionic liquid 1O2O2-Im-2O1 TFSI was performed using a mixture of N-alkoxy imidazole

(1O2O2Im), 2-methoxyethyl iodide (1O2-I) and acetonitrile (1:1.5:4) in Ar/N_2 atmosphere in microwave teflon vials. The sample was microwave irradiated by controlled temperature programming at 150 °C by 2 min ramp and held for 40 min at 150 °C, under a limiting pressure of 18 bar and 500 W power. The reaction progress was monitored by TLC, and ^{1}H NMR from the aliquot. After completion of reaction, the reaction mixture was concentrated via rotavac. A viscous precipitate was obtained by dropwise addition of residue in cold ether. The biphasic system was kept at 0 °C for 2 h. Ether layer was decanted and the residue washed with cold ether. The yellow viscous liquid was subsequently dried in vacuum at 60 °C. The obtained product was then placed for anion exchange with LiTFSI at ambient temperature in acetone. After completion of reaction the product was washed several time with water and the halide ion concentration was anticipated by $AgNO_3$ test. Ionic liquid containing siloxane and ether substituent has been prepared similarly by adding iodomethyldimethyldisiloxane. Propylene carbonate (PC), (TCI 98%), LiTFSI, (TCI, 98%) were used as received without further purification. The electrolyte samples and LiTFSI was evacuated prior to their utilization. The moisture content in the electrolyte samples was eventually found to be below 400 ppm as determined by Karl Fisher titration. The blended electrolyte samples viz., respective (IL + PC) was prepared by addition of 45 mol% of IL in PC and (IL + PC + LiTFSI) by adding 1 mol of LiTFSI/kg of (IL + PC) electrolyte mixture and sonicated at room temperature for 30 min.

2.2 Physical characterization

Thermal stability of the electrolytes was determined by a "TGA/DSC 1" instrument with SDTA sensor from Mettler Toledo upon loading over alumina pan and heating from 30 °C to 800 °C at a heating rate of 10 °C/min under N_2 atmosphere. Determination of the liquid range of ILs was done by differential scanning calorimetry (DSC) using DSC1/700W instrument with HSS8 sensor from Mettler Toledo controlled by STAR^e 12.1 software. The samples were loaded over Al pan and subjected to a temperature range from –90 to 50 °C for DSC analysis. Viscosity measurements were performed by Lovis 2000M Microviscometer, Anton Paar in the temperature range of 10 °C to 100 °C at 5 °C/min heating rate under inert atmosphere.

2.3 Electrochemical measurements

Electrochemical measurements were performed using an Autolab 302N modular potentiostat/galvanostat having FRA32M module for impedance measurements, controlled by Nova 1.11 software in a three-electrode thermostat jacketed electrochemical cell (20 and 50 mL) wrapped in an inert glove bag while being connected with water bath. Glassy carbon (GC) disk (Ø 3 mm) working electrode was utilized along with graphite counter electrode and Ag/Ag^+/PC non-aqueous reference electrode as probe. Before analysis, GC was polished to attain a mirror finish over Nylon polishing cloth (SM 407052, AKPOLISH) by different grades of alumina paste (3, 1, 0.3, 0.05 µm respectively, Pine Instrument, USA) followed by thorough washing and ultrasonication to remove impurities and alumina paste. The experiments were conducted under Ar atmosphere and the electrolytes were purged for 60 min. before starting the experiment and above the electrolyte during the measurement. Impedance measurement was carried out by applying a DC potential over and above an AC perturbation of 10 mV for variable frequencies ranging from 0.1 Hz to 100 kHz in a logarithmic step.

Battery performance and the stability test of ether-ether IL was tested by compiling a lithium-ion cell consisting of graphite anode and $LiCoO_2$ cathode. The anode comprised of 90 wt% graphite (Sigma Aldrich), 4 wt% carbon black (Duralyst) and 6 wt% PVdF binder dissolved in N-methylpyrrolidone (NMP, Alfa Aesar) coated over copper current collector. Whereas, 75 wt% $LiCoO_2$ (Alfa Aesar), 18 wt% carbon black and 7 wt% PVdF in NMP served as cathode slurry over aluminium current collector. A Whatman^{TM} separator was soaked in the ether-ether IL and sandwiched between anode and cathode and their performance was measured galvanostatically at 1C rate (w.r.t cathode) in the potential range of 2.8-4.2 V. The cell was cathode limited with anode to cathode active mass ratio of 1.8 and was assembled in an argon-filled glove box (<2 ppm H_2O, <2 ppm O_2).

2.4 Self-diffusion measurements by PGSE NMR

2.4.1 Sample Preparation

For PGSE-NMR, samples were prepared at ambient temperature in inert atmosphere. The IL, PC and LiTFSI were taken according to ratios taken in the impedance spectroscopy samples, i.e. 1 mol of LiTFSI in 1 kg electrolyte (45:55 molar ratio of IL:PC). For NMR measurements, electrolyte sample was placed into a 5 mm wide NMR tube to a height of 1.8 to 5.8 cm.

2.4.2 NMR Measurements

The PGSE-NMR measurements were made by using a JEOL JNM ECS-400 spectrometer with a 9.4 T wide bore superconducting magnet controlled by JEOL console equipped with JEOL pulse field gradient probes. The self-diffusion coefficients were obtained at 25 °C. The gradient strength was calibrated and cross-checked using the known self-diffusion coefficient of H_2O at 25 °C (2.27 X 10^{-9}).[24] The measurement of self-diffusion coefficient for the imidazolium cation, TFSI anion, and the Li-ion were made by ^{1}H, ^{19}F, and ^{7}Li NMR at frequencies of 399.78 MHz, 376.17 MHz and 155.37 MHz, respectively. All NMR experiments were carried out without sample spinning to prevent disturbance from sample motion. The T1 and T2 measured by inversion recovery as simple spin-echo pulse sequence (180°–Tou–90°–Tou–Aqu) and (90°–Tou–180°–Tou–Aqu) respectively used for the diffusion measurements. The diffusion-ordered NMR spectroscopy (DOSY) was taken by PFG BPPLED experiment, where pulse sequence was (90°–180°–90°–Aqu). The echo signal attenuation (*E*), is related to the experimental parameters by[25]:

Table 2. Electrochemical stability window (ESW) at various temperatures.

Electrolytes	Electrochemical stability window (V)				
	10 °C	25 °C	40 °C	50 °C	60 °C
Ether-ether IL	4.7	5.0	5.0	4.9	4.7
Ether-ether IL + PC	4.8	4.8	4.6	4.6	4.7
Ether-ether IL + PC + LiTFSI	5.6	5.9	5.7	5.6	5.4
Ether-siloxane IL	5.5	5.5	5.5	5.3	5.2
Ether-siloxane IL + PC	5.9	5.7	5.6	5.8	5.6
Ether-siloxane IL + PC + LiTFSI	4.0	4.2	4.1	4.0	4.0

$$\ln(E) = \ln\left\{\frac{S}{S_{g-0}}\right\} = -\gamma^2 g^2 D \delta^2 \left\{\Delta - \frac{\delta}{3}\right\}$$

where D is the diffusion coefficient, S is the spin-echo signal intensity, δ is the duration of the field gradient with magnitude g, γ is the gyromagnetic ratio, and Δ is the interval between the two gradient pulses. Typical acquisition parameters (Δ) 200 ms and (g) 0.003 to 0.28 (1H), 0.03 to 0.28 (^{7}Li), and 0.003 to 0.28 (^{19}F) T/m. The 90° pulse lengths were 10.42 (1H), 10.0 (^{7}Li), and 11.0 (^{19}F) µs. In all cases, a spectral width was digitized into 16K data points. Each spectrum was taken from the average of 5 different δ values from 2 to 6 ms. A full relaxation of 7 s (i.e., >5T1) was used. All the measured signal attenuations were well described by a straight line as expected for free diffusion, and the standard deviations of the plots were less than 1% (^{1}H), 2% (^{19}F) and 10% (^{7}Li).

3 Results and discussion

3.1 Electrochemical Stability

Applicability of ionic liquid electrolytes in the electrochemical devices is profoundly governed by their ability to withstand the working potential range. A relatively reliable means to detect the potential range of stability is by performing either linear sweep or cyclovoltammetry. In the present text, electrochemical stability of two ILs as electrolyte viz., ether-ether and ether-siloxane ILs at variable temperatures along with their respective blends with PC and LiTFSI salt as an electrolyte was determined by performing a series of electrochemical experiments such as LSV, CV and EIS measurements. Both the ether-ether IL and ether-siloxane IL, (IL + PC) and (IL + PC + LiTFSI) electrolytes (Table 1) were subjected to potentials ranging from 3.5 to –5.0 V at a scan rate of 50 mV/s as illustrated in Figure 1. The anodic and the cathodic limits were determined as the point of intersection of the mean line where current as a function of voltage was nearly constant and the oxidative and reductive sections respectively, representing the electrochemical stability window for each of the analyzed ILs and their composite mixtures. The limit of electrochemical stability window [ESW/(voltage stability window)] was extracted from LSV studies (Figure 1) and the effect of temperature over these electrolytes have been displayed in Table 2 and detailed in Table S1 [supporting information (SI)].

Anion oxidation and cation reduction potentials govern the anodic and cathodic limit of the electrochemical window, respectively. Figure 1 shows the LSV of two neat ILs ether-ether IL and ether-siloxane IL at 25 °C having anodic potential limit (AL) of 1.98 V and 2.48 V respectively, indicating ether-siloxane IL is more positive if compared to ether-ether IL, but exhibiting similar cathodic potential limit (CL) of –3.08 V and –3.07 V respectively. This could be due to the Si d-orbital, which possibly houses the incoming electrons, thereby extending the cathodic limit of ether-siloxane IL *vs* the ether-ether IL for neat ILs. Thus, the overall electrochemical window was found to be of 5.06 and 5.55 V for ether-ether IL and ether-siloxane IL, respectively.

However, after addition of PC, AL (1.83 V) potential shifts cathodically and CL (–2.97 V) potential shifts anodically compared to neat IL in the case of ether-ether IL whereas vice-versa was observed for ether-siloxane IL, i.e. AL (2.59 V) and CL (–3.16 V). However, addition of LiTFSI to ether-ether IL leads to an increase in both AL (2.48 V) and CL (–3.47 V), but surprisingly the reverse trend had been observed for ether-siloxane IL (AL: 2.20 V and CL: –2.01 V), indicating less electrochemical stability as compared to ether-ether IL, which is clearly witnessed by its ESW of 5.95 V and 4.21 V upon addition of LiTFSI for ether-ether and ether-siloxane IL, respectively. The noticeable difference in stability could be due to aggregation being more pronounced for the case of ether-siloxane IL, which leads to the exposure of cation upon Li-ion inclusion. This is further supported by self-diffusion studies using NMR. In addition these results are well complimented with the conductivity studies discussed in the forthcoming sections, whereby the conductivity is only 0.5 mS/cm for ether-siloxane IL compared to 2.2 mS/cm for ether-ether IL at 25 °C in presence of high concentration of LiTFSI i.e., 1 mol LiTFSI/kg solvent (Table 3).

Furthermore, the performance of both the IL electrolytes were correlated by varying the temperature which limited the ESW. Hence, the detailed experiments were carried out for neat ILs, ILs and PC, and upon addition of LiTFSI to ILs and PC, the results obtained are tabulated in Table S1 (SI) and represented in Figure S1 (SI). As observed from Table S1 (SI), for ether-ether IL, with increase in temperature up to 40 °C the CL increases, however further increase in temperature tended to decrease both CL and AL and similar trend had also been observed in the case of ether-siloxane IL. On the other hand, in the case of ether-ether IL upon addition of LiTFSI both CL and AL potential decreases with increase in temperature except at 10 °C wherein AL potential is much lower compared to the temperatures above 25 °C. Interestingly, both CL and AL

potential are higher than that of neat IL in the entire temperature range. Moreover, for ether-ether IL with increase in temperature from 10 to 40 °C, the ESW tended to increases from 4.76 V to 5.08 V. However, further increase in the temperature above 40 °C causes a small decrease in ESW in the order of 200 to 400 mV compared to lower temperature range.

Although, ether-siloxane IL and with PC exhibited the similar trend as in ether-ether IL in the entire temperature range, but surprisingly, upon addition of LiTFSI both AL and CL potential decreases compared to neat IL. Thus, the ESW also decreases in the entire temperature range and at 25 °C it decrease from 5.55 V (neat IL) to 4.21 V. This could be due to the variable extent of interaction between these molecular species. For example, ether-ether IL with PC exhibit an ESW close to mixture of PC and LiTFSI (~5.8 V, Figure S2, SI). However, ESW for ether-siloxane IL is much better compare to upon addition of PC and LiTFSI suggesting that the solvation of IL-PC is much stronger in case of ether-siloxane. This can be further realized from the IR stretching frequencies of C=O and S-N-S as shown in Figure S3 and Table S2 (SI).

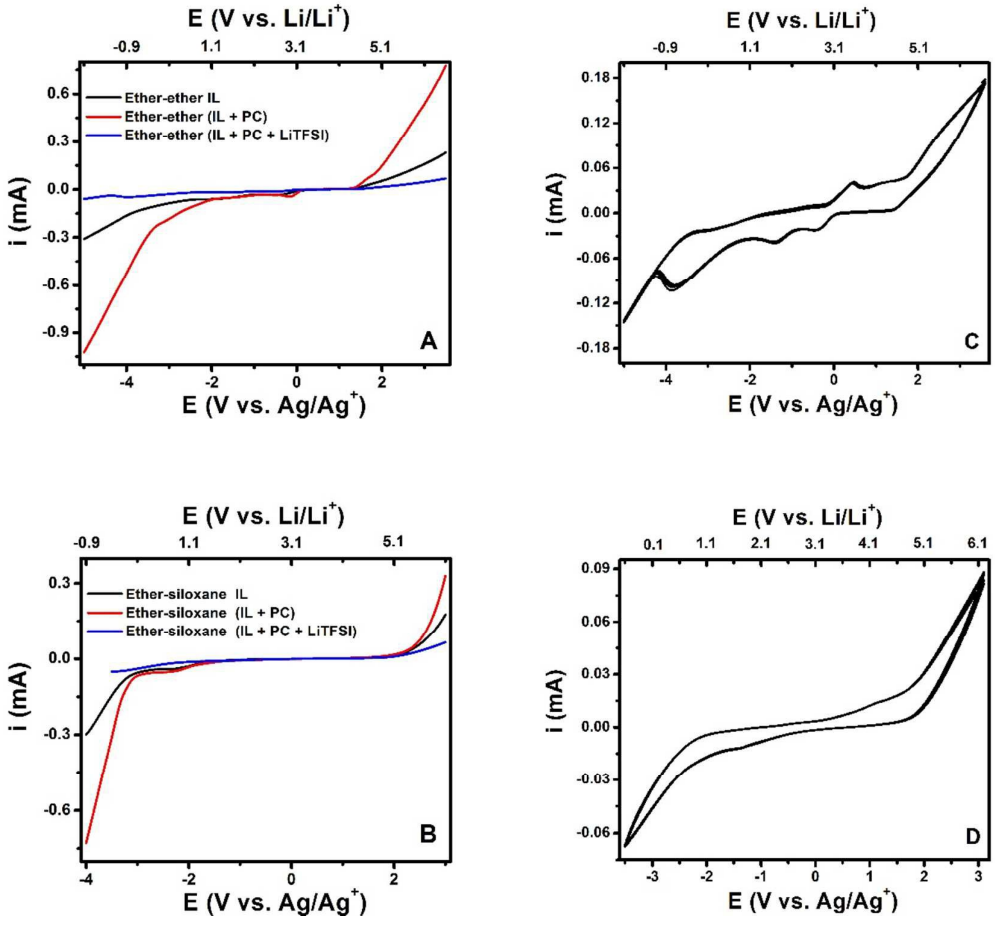

Fig. 1 Linear sweep voltammograms of (A) ether-ether IL, (IL + PC) and (IL + PC + LiTFSI); (B) ether-siloxane IL, (IL + PC) and (IL + PC + LiTFSI) at a sweep rate of 50 mV/s at 25 °C; consecutive cyclovoltammograms depicting nature of ILs after 10 cycles with varying temperatures for (C) ether-ether (IL + PC + LiTFSI) and (D) ether-siloxane (IL + PC + LiTFSI) at a sweep rate of 100 mV/s, WE: glassy carbon (GC), CE: graphite rod, RE: Ag/Ag^+/PC.

The ESW tended to decrease upon addition of PC for ether-ether IL, but increased for ether-siloxane IL, and surprisingly the order gets reversed upon LiTFSI addition. These findings suggest that ether-ether IL emerges out to be relatively more electrochemically stable than ether-siloxane IL even in presence of high concentration of Li-ion due to stronger interactions and cluster formation of Li-ion with IL. Additionally, to evaluate the long term stability of an IL

electrolyte continuous CV experiments were performed at 25 °C with a sweep rate of 100 mV/s and the obtained results are displayed in Figure 1C & 1D and Figure S4 (SI). It can be noticed from Figure 1C and 1D, even after 10 successive cycles, i.e., a time of approximately 90 min, no decay in the CV curves could be observed. Moreover, the experiments were also performed at different temperatures ranging from 10-60 °C for 10 cycles. In the entire temperature range, we did not observe any changes in the behavior of CV curves. An important fact is that even after repeated measurements at 25 °C and after the successive measurements at various temperatures with continuous cycling, nature of curves remains same as observed in the previous measurement at same temperature (Figure not shown) in wide potential range reinforcing their stability. Upon addition of LiTFSI however, the first cycle shows slightly enhanced current compared to the subsequent ones suggesting formation of a thin SEI layer over GC electrode[26] (Figure S4 E and F, SI).

3.2 Impedance analysis

Profound analysis of the presented ILs as electrolyte were performed by employing detailed temperature dependent impedance measurements under half-cell conditions. Impedance gives a dynamic conductivity in terms of coherence with the real complete cell conditions. Thus, impedance analysis of the analyzed IL electrolytes as neat IL, (IL + PC) and (IL + PC + LiTFSI) at variable potentials and temperatures would substantially gauge their applicability as electrolyte in battery systems. First series of experiments were conducted at various potentials in the entire potential range of measured ESW. Figure S5 (SI) depicts the Nyquist plot for ether-ether IL electrolytes at 25 °C for variable potentials ranging from –3.0 V to 2.0 V. When

Journal Name

ARTICLE

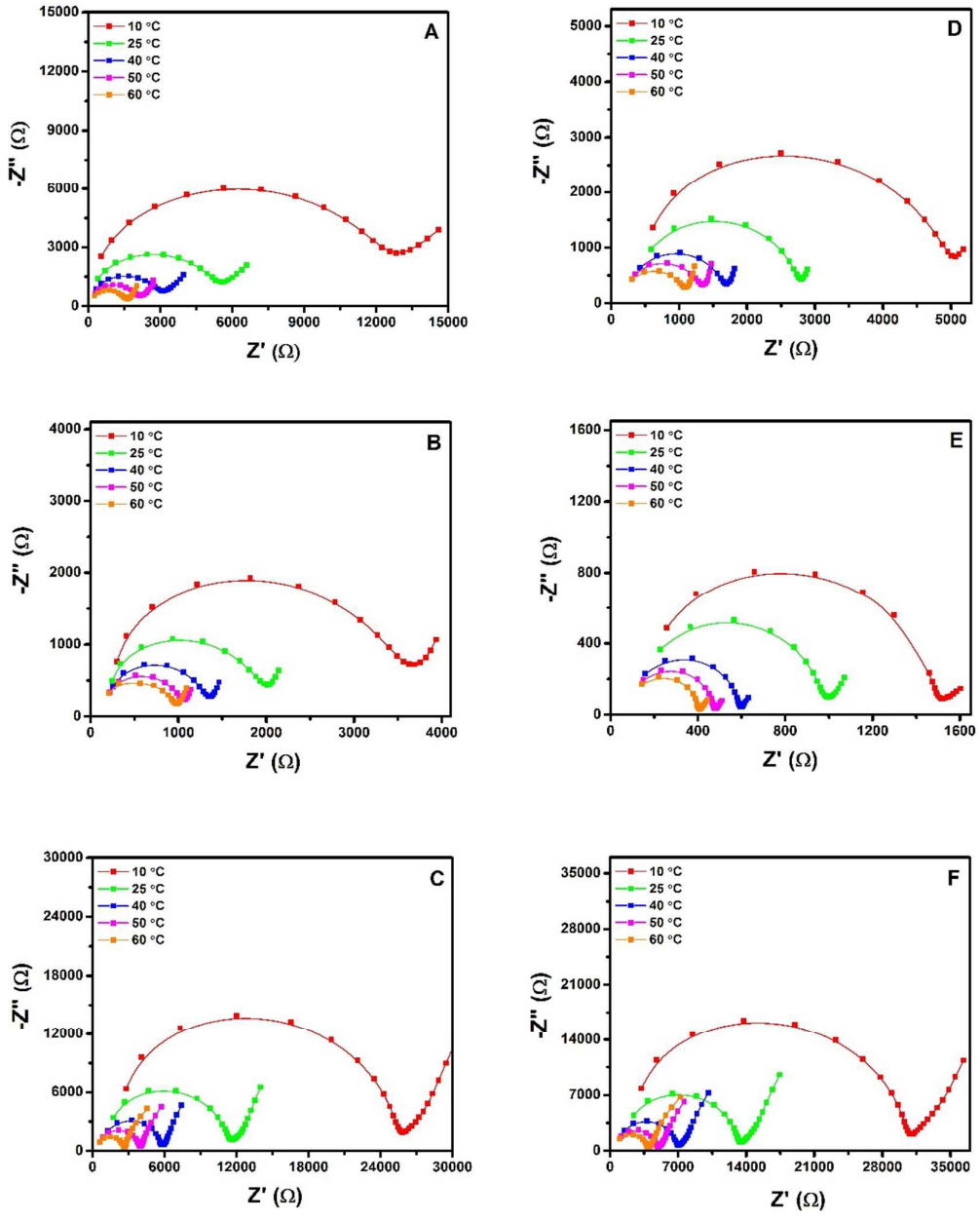

Fig. 2 Impedance response of (A) ether-ether IL; (B) ether-ether IL + PC; (C) ether-ether IL + PC + LiTFSI, performed in 20 mL jacketed glass cell (7.07 cm^{-1} cell constant); and (D) ether-siloxane IL; (E) ether-siloxane (IL + PC); (F) ether-siloxane IL + PC + LiTFSI, performed in 50 mL jacketed glass cell (25.1 cm^{-1} cell constant) at 25 °C, WE: glassy carbon (GC), CE: graphite rod, RE: Ag/Ag^{+}/PC.

frequencies were varied from 0.1 Hz to 100 kHz, the analysis results in a semicircular behavior at the high frequency region and a stout tail towards low frequency. As expected, no deviation in the semicircle behavior was observed at the measured potentials indicating that varying the potential has negligible effect over the impedance behavior of the analyte. This is so since impedance remains same in the span of the electrochemical window of the electrolyte, whereby uniformity is attained as resistance for Li-ion migration through surface films is supposed to be potential-independent.[27] The only difference observable is at low frequency range depicting Warburg diffusion in presence of LiTFSI, indicating variation in the diffusion behavior of Li-ion.[28] Solution resistance (R_s) is marked by the intersection of the semicircle with real axis in the high frequency region and the one in the low frequency region amounts to polarization resistance (R_p) near the electrode

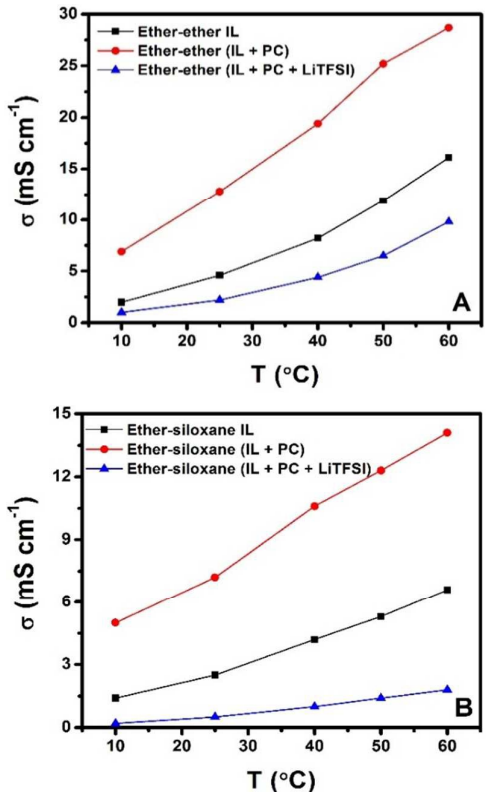

Fig. 3 Temperature dependence of ionic conductivity of (A) ether-ether IL, (IL + PC) and (IL + PC + LiTFSI); (B) ether-siloxane IL, (IL + PC) and (IL + PC + LiTFSI) extracted from impedance analysis.

Interface.[29-30] Difference between R_p and R_s results in the charge transfer resistance (R_{ct}), which is directly related to the conduction of Li-ion to the electrode successfully. The diameter of the semicircle (R_{ct}) was almost constant upon potential variation as conductivity remains same at a particular temperature. Conductivity of ILs at different temperatures was determined by making use of the cell constant and the impedance derived R_{ct} value. As observed from Figure S5 (SI), there is no decay/change in semicircle behavior in the respective IL and their composites electrolyte even at different applied DC potential. Based on the above results, potential of –2.0 V was chosen for further temperature-dependent impedance analysis experiments. Figure 2 represents the impedance responses of both ILs, their composites and upon addition of LiTFSI. As it is clear from Figure 2A-C, for ether-ether IL with increase in temperature from 10 to 60 °C, decrease in behavior of semi-circle was observed i.e., resistance decrease which in turn increases the conductivity. The conductivity value varies from 2.0 to 16.1 mS/cm for a temperature ranging from 10-60 °C. However, upon addition of PC the conductivity increases to 6.9-28.7 mS/cm (10-60 °C). As expected, addition of LiTFSI leads to decrease in conductivity from 1.0-9.8 mS/cm. This could be due to the formation of solvation cluster which in turn leads to high viscosity and low diffusion of IL, as well as Li-ion as confirmed by self-diffusion study (discussed in forthcoming section). The ether-siloxane IL (Figure 2D-F) also follows the same trend as in the case of ether- ether IL except the decrease in conductivity compared to ether-ether IL. Additionally, Warburg diffusion behavior was observed for LiTFSI containing composite mixture. This suggested that thermal effects sets in rapid molecular motions, lowering the viscosity while enhancing shuttling efficiency of the medium for Li-ions. Ether-siloxane IL and its mixture with PC and upon addition of PC with LiTFSI also tend to display similar behavior of increased conductivity upon increasing the temperature. Quantitative account of conductivities for both ether-ether and ether-siloxane ILs and their respective mixtures are compiled in Table 3. The conductivity trend obtained from Table 3 upon addition of PC and then additionally LiTFSI along with IL and PC is supported by self-diffusion coefficient and viscosity measurements. These aspects are detailed in the upcoming sections. The variation of conductivity measured by impedance spectroscopy by virtue of temperature is summarily represented by Figure 3. The conductivity tended to increase upon increasing the applied temperature due to thermal convection effects which sets in ionic motions.

Table 3. Conductivity data of various electrolytes extracted from impedance analysis at different temperatures.

Electrolytes	Conductivity (mS/cm)				
	10 °C	25 °C	40 °C	50 °C	60 °C
ether-ether IL	2.0	4.6	8.2	11.9	16.1
ether-ether IL + PC	6.9	12.8	19.4	25.2	28.7
ether-ether IL + PC + LiTFSI	1.0	2.2	4.4	6.5	9.8
Ether-siloxane IL	1.4	2.5	4.2	5.3	6.6
Ether-siloxane IL+ PC	5.0	7.2	10.6	12.3	14.1
Ether-siloxane IL + PC + LiTFSI	0.2	0.5	1.0	1.4	1.8

Conductivity measurement via impedance analysis indicates that ether-ether IL exhibits appreciable conductivity at 25 °C compared to the ether-siloxane IL and the previously reported literature,[18,21,31-36] which further increases upon increasing the temperature. Thus, ether-ether IL could be employed as an efficient electrolyte, which is redox-robust over a potential range (ESW) of 5.9 V and highly conductive in presence of PC (55 mol%) and LiTFSI (1 mol/kg electrolyte) at 25 °C.

3.3 Battery performance

Further, to evaluate the battery performance and the stability test, measurements were carried out by compiling a lithium-ion cell comprising of ether-ether IL electrolyte drenched Whatman separator sandwiched between graphite anode and $LiCoO_2$ cathode. The experiment were carried out galvanostatically to observe the formation of SEI layer and it's cycling stability.

The voltage profile for charge-discharge is represented in Figure S6A (SI), the foremost discharge capacity obtained was 85.7 mAh/g, and this then subsequently dropped down to 39.4 mAh/g for the 10^{th} cycle and stabilized at 37.9 mAh/g after 50 cycles. The drastic change in the discharge capacity from the first and subsequent cycles could be ascribed to the formation of the protective solid electrolyte interphase (SEI) preventing further capacity loss in the cell and stable performance by the battery till 50 cycles. Figure S6B (SI), represents the variation of discharge capacity with the passage of charge-discharge cycles and as evident the assessed ether-ether IL electrolyte is stable in the measured 50 cycles. Thus, the assembled full cell with ether-ether IL electrolyte turned out to be stable with moderate capacity and stability which could be further optimized to enable improved performance.

3.4 Viscosity and self-diffusion studies

The resistance to flow of ions in the ILs and their mixtures were measured under inert atmosphere against temperature variation from 10-100 °C. Figure S7 (SI) represents the viscosity variation for neat IL, (IL + PC) and (IL + PC + LiTFSI) for both ether-ether IL and ether-siloxane ILs. It clearly depicts that viscosity decreases upon addition of PC (Table S3, SI) as expected, but then shoots up upon further addition of LiTFSI. The trend remains the same for both the ILs tested, but still ether-ether IL is substantially less viscous in presence of PC and Li-ion. Thereby, ether-ether IL is expected to be more efficient in shuttling Li-ion. This could be due to the presence of ether group in IL which inhibits deleterious phenomenon like self-aggregation between cation and anion while promoting polarity and ion solvation.[13, 37-38]

These analysis reflects the fact that addition of PC increases the conductivity while viscosity of the composite goes down. This is ascribable to the strong solvating ability of organic carbonates and their better mobility.[39] Furthermore upon addition of LiTFSI salt, the viscosity increases bringing down its conductivity due to increment in the concentration of anion which interacts electrostatically with Li-ion, resulting in its diminished mobility.[21,35,40] Hayamizu *et al*,[33] have also reported that the activation energy required upon increasing the concentration of Li-ion tends to increase due to reduced mobility. Another probable reason is that the TFSI anion contributes towards solvation of Li-ion leading to the formation of $Li[TFSI]_{n+1}^{n-}$ species whose migration towards negative electrode is dominated by both concentration and potential gradient as a result of being negatively charged. The solvated Li-ion moves towards the anode only when the concentration gradient dominates over the potential gradient.[41] All of the above mentioned factors contribute to the decreased conductivity upon addition of a high concentration (1 mol/kg solvent) of LiTFSI salt. High concentration of Li salt was used in this study to demonstrate the stability of these IL electrolytes (IL+PC+LiTFSI). As seen in Figure 2 and Table 3, the conductivity decreases drastically in both ILs after the addition of LiTFSI from 2 to 1.0 mS/cm and 1.4 to 0.2 mS/cm for ether-ether IL and ether-siloxane IL, respectively. However, it is known fact that with increasing concentration of Li-salt the viscosity increases which in turn decreases the conductivity due to strong solvation of Li-ion in IL and PC.[42] The effects of solvation and mobility of ions on conductivity can be further justified by self-diffusion studies of these ions.

Table 4 shows the self-diffusion coefficient for $[Imd]^+$, $[TFSI]^-$, Li^+ species in different mixtures of electrolytes (neat IL, IL and LiTFSI, and composites of IL with LiTFSI and PC) at 25 °C. It is clear from Table 4, that the diffusion coefficient of both $[Imd]^+$ and $[TFSI]^-$ in case of ether-ether IL is higher compared to that of ether-siloxane IL. As expected in all cases, the $[TFSI]^-$ has largest diffusion coefficient despite of the higher molecular weight of cation. Further, upon addition of LiTFSI the mobility of all the ions is restricted, which is clear from its diffusion coefficient, presumably due to the addition of Li-ion which decreases the fluidity of the entire system. Hence, all species in the mixture of IL and LiTFSI show a decreased diffusivity. However, the restriction is more pronounced in ether-siloxane IL leading to the decrease of total diffusion (D_{SUM}) by ~8 times in ether-siloxane IL compared to that of ether-ether IL which is only about ~6 times. This is attributed to the aggregation of Li-ion that is much pronounced in ether-siloxane IL in presence of LiTFSI. Whereas in case of ether-ether IL the presence of ether

groups on both side of $[Imd]^+$ produces enough flexibility and also interact with Li-ion which helps to accommodate more Li-ion which in turn aids to collapse LiTFSI cluster.

But the scenario is completely different after the addition of PC to the mixture of IL and LiTFSI and mobility of all the species were recovered. As expected in both the IL composites (IL, PC and LiTFSI) Li-ion diffusion is slowest and the PC diffusion is fastest. The relative increase in diffusion coefficient was especially pronounced for Li-ion, in line with the trends found for the effect of solvent addition on the conductivity of the electrolyte. Flexible ether groups with oxygen atoms give strong interaction with Li-ion. Ether-ether IL with both side ether groups interact with Li^+ much stronger than in ether-siloxane IL. Due to this strong interaction $Li[TFSI]_{n+1}^{n-}$ cluster formation is less favourable in ether-ether IL, hence the effective Li^+ radius is less and mobility of Li-ion is more than in the case of ether-siloxane.

The above analysis was further supported by IR studies. As can be seen from Figure S3 and Table S2 (SI), C=O stretching of neat PC increased upon addition of ILs from 1786 to 1788/1791 cm^{-1} for ether-ether and ether-siloxane, respectively, which indicates breaking of PC aggregation and again goes back to 1786 cm^{-1} in PC+IL+LiTFSI composites of both ILs. Due to the direct interaction of TFSI anion with imidazolium cation and/or Li-ion the shift is more pronounced in stretching frequency of S-N-S. For example, $\nu_{S\text{-}N\text{-}S}$ peak at 789 cm^{-1} shifted to lower wavenumber to 777 cm^{-1} upon addition of PC for both ILs, which shows that the TFSI is almost free from interaction with imidazolium cation. Similarly, $\nu_{S\text{-}N\text{-}S}$ peak shifted to higher wavenumber, ca. 794 cm^{-1}, upon addition of LiTFSI due to strong interaction with Li-ion. The interaction is much stronger in ether-siloxane IL and more TFSI is involved in cluster formation. However, the $\nu_{S\text{-}N\text{-}S}$ peak again shifted to lower frequency, ca. 787 cm^{-1} in (IL+PC+LiTFSI) composite, indicating that TFSI is partially free and the interaction is almost similar in both ILs.

3.5 Thermal Stability

Thermal stability is an important aspect of concern for electrolytes as it dominates their overall stability and applicability. Determination of the temperature stability range and its phase transitions aids in appropriate selection of electrolytes based on their site or device of application. In lithium and Li-ion batteries the electrolytes are expected to have a low crystallization or glass transition temperature (T_g)

Table 4. Self-diffusion coefficient of ether-ether and ether-siloxane ILs and their mixtures (IL+LiTFSI, IL+PC+LiTFSI) at 25 °C

IL	Self-diffusion coefficient (m^2/s)		
	$[Imd]^+$ (^1H)	TFSI (^{19}F)	Li^+ (^7Li)/PC (^1H)
ether-ether IL	4.16	4.52	--
ether-ether IL + LiTFSI	0.32	0.96	0.08
ether-ether IL + PC + LiTFSI	2.12	1.14	0.52 /4.60
Ether-siloxane IL	3.76	4.49	--
Ether-siloxane IL + LiTFSI	0.31	0.56	0.11
Ether-siloxane IL + PC + LiTFSI	1.98	1.89	0.25 / 4.08

Self-diffusion coefficient (by ^1H and ^{19}F) X 10^{-11} (m^2/s) at 1.0 mol/kg LiTFSI

and simultaneously very high thermal decomposition temperature (T_{start}). These features render the device operational over a wide range of temperature and reduced risk of thermal runaways and explosions. Hence, detailed thermal gravimetric analysis (TGA) was performed for both the ether-ether and ether-siloxane ILs as neat and in combination with PC (55 mol%) and LiTFSI (1 mol/kg solvent) under inert atmosphere for temperatures ranging from 30 to 800 °C at the rate of 10 °C/min.

As seen from Figure 4, the neat IL and IL in combination with LiTFSI undergoes 90% of weight loss in the temperature range of 350 to 530 °C, while IL with PC and IL in combination with PC and LiTFSI undergoes weight loss via two major steps. Initially 15% weight loss was observed up to 246 °C, this could be accounted to the loss of less stable PC component, while the major weight loss of 75% in the second step was due to the IL. As clearly illustrated in Figure 4, decomposition was not observed below 100 °C, for both ILs and they also possess a high T_{onset} of ~150 °C compared to the reported ones.[32]

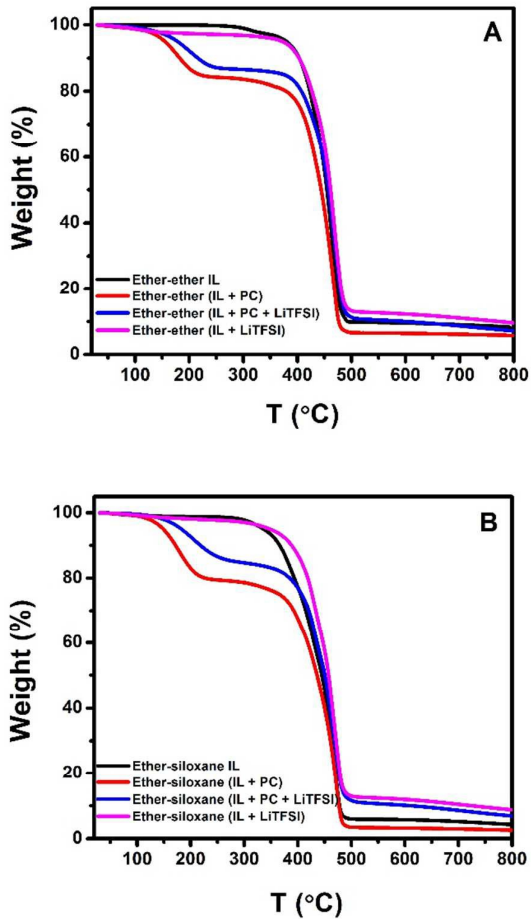

Fig. 4 TGA analysis of (A) ether-ether IL, (IL + PC), (IL + PC + LiTFSI) and (IL + LiTFSI); (B) ether-siloxane IL, (IL + PC), (IL + PC + LiTFSI) and (IL + LiTFSI).

This signifies that PC inclusion results in the operational range limits below 100 °C, whereas that for neat IL and (IL with LiTFSI) shoots up to ~350 °C. Another interesting aspect is that, upon addition of LiTFSI to the mixture of IL and PC an enhancement in the T_{start} was observed from 110.5 to 150.6 °C for ether-ether and from 103.7 to 130.8 °C for ether-siloxane ILs, respectively. Simultaneously, the (IL with LiTFSI) also exhibited an enhanced T_{start} form 309.7 to 355.9 °C and 307.4 to 329.0 °C for ether-ether and ether-siloxane, respectively, compared to that of neat ILs.[43] These observations support the fact that ether-ether substituent over $[Imd]^+$ prizes comparatively better thermal stability over the ether-siloxane under similar circumstances.

Further, in order to evaluate the lower temperature range of ILs and their respective mixtures for fruitful application as an electrolyte, differential scanning calorimetry (DSC) measurement was performed in the temperature range of –90 to 20 °C at a rate of 5 °C/min. The resulting phase transitions are depicted in Figure 5 and the elaborated data is presented in Table S4 (SI) summarizing the variation in glass transition temperature (T_g) for both the ILs and their respective composite mixtures.

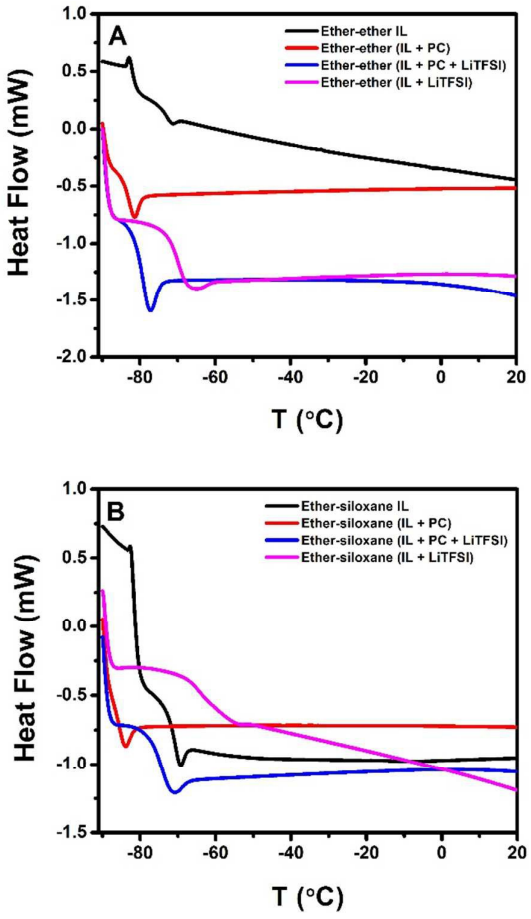

Fig. 5 DSC thermogram for (A) ether-ether IL, (IL + PC), (IL + PC + LiTFSI) and (IL + LiTFSI); (B) ether-siloxane IL, (IL + PC), (IL + PC + LiTFSI) and (IL + LiTFSI).

As observed from Figure 5, the crystallization temperature has not been attained in the measured range of temperature, instead it exhibits amorphous behavior with T_g below –70 °C. Only one peak was observed during the heating scan while none in the reverse scan. However, T_g tends to reduce when PC was mixed with the ILs, but upon addition of LiTFSI increase in T_g was observed compared to that for the (IL + PC) mixture while still being less than that for the neat ILs. Moreover, addition of Li-ion to the ILs, small increase in T_g was observed owing to increased viscosity. The ether-ether functionality imparts low phase transition temperature in all the composite mixtures than the ether-siloxane one due to flexibility which in turn reduces the ion symmetry. The above mentioned is ascribable to the electrostatic interactions between oxygen-atom of ether substituents and the large imide anion.[44] These thermal properties of ether-containing ILs are dominated by their high flexibility, decreased lattice energy on account of

lower symmetry and their packing in lieu of repulsive interactions between neighbouring oxygen-atoms.[36]

4 Conclusions

Ether and siloxane functionalized imidazolium ILs and their mixture with 55 mol% propylene carbonate have been scrutinized in the present study for their temperature-dependent electrochemical analysis for potential application as an electrolyte in lithium and lithium-ion batteries. The temperature-dependent electrochemical impedance spectroscopy (EIS) was performed in a half-cell reaction for mimicking the complete cell conditions to gauge its suitability as battery electrolyte. Both the imidazolium-based electrolytes presented exemplify desirable thermal and electrochemical characteristics. Ether-ether IL nonetheless exhibits comparatively better aspects in terms of Li-ion conducting ability and electrochemical stability window (ESW) in presence of Li-ion compared to ether-siloxane IL. It seems the ether functionality on imidazolium cation is particularly beneficial which interact with Li-ion and helps to collapse the $Li[TFSI]_{n+1}^{n-}$ cluster, and plays important role in the Li-ion mobility. In IL+PC+ LiTFSI mixture the conductivity, viscosity or diffusion is controlled by both PC and the functionalized imidazolium cations. These results show that using mixtures of IL and PC it is possible to achieve high performance also when a large amount of ILs and a high concentration of Li-ion (1 mol/kg) are present inside the electrolyte. Further, full cell measurement shows the moderate capacity and stability of ether-ether IL electrolyte which pose themselves as a potential candidate for electrolyte application in battery systems.

Acknowledgements

This research is supported by the Department of Atomic Energy (DAE), India (2013/37C/57/BRNS). Dr. Tharamani C. Nagaiah thanks Department of Science and Technology (DST) for Ramanujan Fellowship (SR/S2/RJN-26/2012). Santosh N. Chavan thanks to UGC and Aarti Tiwari thanks IIT Ropar for Fellowship.

References

1 Zhou, H.; Wang, Y.; Li, H.; He, P., *ChemSusChem*, 2010, **3**, 1009-1019.
2 Zhou, G.; Li, F.; Cheng, H.-M., *Energy Environ. Sci.*, 2014, **7**, 1307-1338.
3 Scrosati, B.; Hassoun, J.; Sun, Y.-K., *Energy Environ. Sci.*, 2011, **4**, 3287-3295.
4 Tarascon, J. M.; Armand, M., *Nature*, 2001, **414**, 359-367.
5 Etacheri, V.; Marom, R.; Elazari, R.; Salitra, G.; Aurbach, D., *Energy Environ. Sci.*, 2011, **4**, 3243-3262.
6 Lewandowski, A.; Świderska-Mocek, A., *J. Power Sources*, 2009, **194**, 601-609.
7 Goodenough, J. B.; Park, K.-S., *J. Am. Chem. Soc.*, 2013, **135**, 1167-1176.
8 Choi, N.-S.; Chen, Z.; Freunberger, S. A.; Ji, X.; Sun, Y.-K.; Amine, K.; Yushin, G.; Nazar, L. F.; Cho, J.; Bruce, P. G., *Angew. Chem., Int. Ed.*, 2012, **51**, 9994-10024.
9 Wang, Y.; Zaghib, K.; Guerfi, A.; Bazito, F. F.; Torresi, R. M.; Dahn, J., *Electrochim. Acta*, 2007, **52**, 6346-6352.
10 Yoon, H.; Lane, G.; Shekibi, Y.; Howlett, P.; Forsyth, M.; Best, A.; MacFarlane, D., *Energy Environ. Sci.*, 2013, **6**, 979-986.
11 MacFarlane, D. R.; Tachikawa, N.; Forsyth, M.; Pringle, J. M.; Howlett, P. C.; Elliott, G. D.; Davis, J. H.; Watanabe, M.; Simon, P.; Angell, C. A., *Energy Environ. Sci.*, 2014, **7**, 232-250.
12 Armand, M.; Endres, F.; MacFarlane, D. R.; Ohno, H.; Scrosati, B., *Nat. Mater.*, 2009, **8**, 621-629.
13 Quartarone, E.; Mustarelli, P., *Chem. Soc. Rev.*, 2011, **40**, 2525-2540.
14 Guerfi, A.; Dontigny, M.; Charest, P.; Petitclerc, M.; Lagacé, M.; Vijh, A.; Zaghib, K., *J. Power Sources*, 2010, **195**, 845-852.
15 Lombardo, L.; Brutti, S.; Navarra, M. A.; Panero, S.; Reale, P., *J. Power Sources*, 2013, **227**, 8-14.
16 Tsuda, T.; Kondo, K.; Tomioka, T.; Takahashi, Y.; Matsumoto, H.; Kuwabata, S.; Hussey, C. L., *Angew. Chem.*, 2011, **123**, 1346-1349.
17 Goodenough, J. B.; Kim, Y., *Chem. Mater.*, 2009, **22**, 587-603.
18 Vogl, T.; Menne, S.; Balducci, A., *Phys. Chem. Chem. Phys.*, 2014, **16**, 25014-25023.
19 Kühnel, R.-S.; Balducci, A., *J. Phys. Chem. C*, 2014, **118**, 5742-5748.
20 Montanino, M.; Moreno, M.; Carewska, M.; Maresca, G.; Simonetti, E.; Presti, R. L.; Alessandrini, F.; Appetecchi, G., *J. Power Sources*, 2014, **269**, 608-615.
21 Chavan, S. N.; Mandal, D., *RSC Adv.*, 2015, **5**, 64821-64831.
22 R. Yanagisawa, H. Endo, M. Unno, H. Morimoto and S.-i. Tobishima, *J. Power Sources*, 2014, **266**, 232-240.
23 A. Sacco, F. Bella, S. De La Pierre, M. Castellino, S. Bianco, R. Bongiovanni and C. F. Pirri, *ChemPhysChem*, 2015, **16**, 960-969.
24 Hayamizu, K.; Aihara, Y.; Arai, S.; Price, W. S., *Electrochim. Acta*, 2000, **45**, 1313-1319.
25 E. Stejskal, *J. Chem. Phys.*, 1965, **43**, 3597-3603.
26 M. Park, X. Zhang, M. Chung, G. B. Less and A. M. Sastry, *J. Power Sources*, 2010, **195**, 7904-7929.
27 Aurbach, D.; Markovsky, B.; Weissman, I.; Levi, E.; Ein-Eli, Y., *Electrochim. Acta*, 1999, **45**, 67-86.
28 Doi, T.; Iriyama, Y.; Abe, T.; Ogumi, Z., *Anal. Chem.*, 2005, **77**, 1696-1700.
29 Yamada, Y.; Iriyama, Y.; Abe, T.; Ogumi, Z., *J. Electrochem. Soc.*, 2010, **157**, A26-A30.
30 Liao, C.; Guo, B.; Sun, X. G.; Dai, S., *ChemSusChem*, 2015, **8**, 353-360.
31 Li, M.; Yang, L.; Fang, S.; Dong, S.; Jin, Y.; Hirano, S.-i.; Tachibana, K., *J. Power Sources*, 2011, **196**, 6502-6506.
32 Wang, H.; Liu, S.; Huang, K.; Yin, X.; Liu, Y.; Peng, S., *Int. J. Electrochem. Sci.*, 2012, **7**, 1688-1698.
33 Hayamizu, K.; Tsuzuki, S.; Seki, S.; Ohno, Y.; Miyashiro, H.; Kobayashi, Y., *J. Phys. Chem. B*, 2008, **112**, 1189-1197.
34 Suematsu, M.; Yoshizawa-Fujita, M.; Tamura, T.; Takeoka, Y.; Rikukawa, M., *Int. J. Electrochem. Sci.*, 2015, **10**, 248-258.
35 Fang, S.; Tang, Y.; Tai, X.; Yang, L.; Tachibana, K.; Kamijima, K., *J. Power Sources*, 2011, **196**, 1433-1441.
36 Ferrari, S.; Quartarone, E.; Tomasi, C.; Ravelli, D.; Protti, S.; Fagnoni, M.; Mustarelli, P., *J. Power Sources*, 2013, **235**, 142-147.
37 Kunze, M.; Paillard, E.; Jeong, S.; Appetecchi, G. B.; Schönhoff, M.; Winter, M.; Passerini, S., *J. Phys. Chem. C*, 2011, **115**, 19431-19436.
38 Branco, L. C.; Rosa, J. N.; Moura Ramos, J. J.; Afonso, C. A. M., *Chem. Eur. J.*, 2002, **8**, 3671-3677.

39 Lee, S.-Y.; Yong, H. H.; Lee, Y. J.; Kim, S. K.; Ahn, S., *J. Phys. Chem. B*, 2005, **109**, 13663-13667.
40 Fromling, T.; Kunze, M.; Schonhoff, M.; Sundermeyer, J.; Roling, B., *J. Phys. Chem. B*, 2008, **112**, 12985-12990.
41 Saito, Y.; Umecky, T.; Niwa, J.; Sakai, T.; Maeda, S., *J. Phys. Chem. B*, 2007, **111**, 11794-11802.
42 Hayamizu, K.; Aihara, Y.; Arai, S.; Garcia, *J. Phys. Chem. B*, 1999, **103**, 519-524.
43 Jin, Y.; Fang, S.; Yang, L.; Hirano, S.-i.; Tachibana, K., *J. Power Sources*, 2011, **196**, 10658-10666.
44 Ferrari, S.; Quartarone, E.; Mustarelli, P.; Magistris, A.; Protti, S.; Lazzaroni, S.; Fagnoni, M.; Albini, A., *J. Power Sources*, 2009, **194**, 45-50.